Computational methods for design of organic materials with high charge mobility

Linjun Wang,[a] Guangjun Nan,[a] Xiaodi Yang,[a] Qian Peng,[a] Qikai Li[a] and Zhigang Shuai*[ab]

Charge carrier mobility is at the center of organic electronic devices. The strong couplings between electrons and nuclear motions lead to complexities in theoretical description of charge transport, which pose a major challenge for the fundamental understanding and computational design of transport organic materials. This *tutorial review* describes recent progresses in developing computational tools to assess the carrier mobility in organic molecular semiconductors at the first-principles level. Some rational molecular design strategies for high mobility organic materials are outlined.

1. Introduction

Semiconducting materials are key building blocks in modern micro-electronics. In the past decade, organic molecular semiconductors have received growing interests for electronic and opto-electronic applications, such as organic field-effect transistors (OFETs), organic light-emitting diodes (OLEDs), organic photovoltaic cells (OPVs) and various types of sensors.[1–4] These possess great advantages such as low cost, easy fabrication, mechanical flexibility, light weight, and large-area production. A crucial characteristic of a semiconductor is the ability to control the electrical conductance. In this respect, the most important quantity in characterizing the charge transport ability is the carrier mobility (μ), which is defined as the ratio between the charge drift velocity (ν) and the driving electric field (F):

$$\mu = \nu/F \qquad (1)$$

Generally, the room-temperature mobility for inorganic semiconductors such as single-crystal silicon can reach as high as 10^2–10^3 cm^2 V^{-1} s^{-1},[5] and for single-walled carbon nanotubes, the mobility can surpass 10^5 cm^2 V^{-1} s^{-1}.[6] Traditionally, organic materials possessed mobilities of around 10^{-5} cm^2 V^{-1} s^{-1},[7] too small for practical applications. Creating functional organic materials with large mobilities is a central challenge in the field of organic electronics. A variety of new materials have been synthesized with mobilities exceeding 0.1 cm^2 V^{-1} s^{-1} in thin films[2] and 10 cm^2 V^{-1} s^{-1} in crystals.[8,9] Although the charge transport mechanism has been studied for several decades,[10–15] the theoretical understanding is still limited, due to the complexities of organic materials and the wide variety of structures.

Ultra-pure organic single crystals, in the absence of chemical impurities and structural disorder, are prototypical systems in

[a] Key Laboratory of Organic Solids, Beijing National Laboratory for Molecular Science (BNLMS), Institute of Chemistry, Chinese Academy of Sciences, Beijing, 100190, People's Republic of China
[b] Department of Chemistry, Tsinghua University, Beijing, 100084, People's Republic of China. E-mail: zgshuai@tsinghua.edu.cn

Linjun Wang was born in Jiangsu, China, in 1982. He graduated with a BS degree from the University of Science and Technology of China in 2004, and then studied in Prof. Zhigang Shuai's group at the Institute of Chemistry, Chinese Academy of Sciences (CAS) and obtained his PhD in 2009. His main research interest includes theoretical modeling of charge transport in organic semiconductors and electronic properties of self-assembled monolayers on metal surfaces.

Linjun Wang

Guangjun Nan was born in Henan, China, in 1981. He received both his BS (2003) and MS (2006) degrees majoring in physics from Jilin University, and received his PhD from the Institute of Chemistry, Chinese Academy of Sciences (Prof. Zhigang Shuai's group) in 2009. His doctoral thesis focused on charge-transfer theory in complex systems and charge mobility in organic materials. Now he is an assistant professor in Harbin Institute of Technology.

Guangjun Nan

which to understand the intrinsic charge transport properties.[9] In such ideal systems, charge transport is limited only by thermal nuclear vibrations, and most theoretical studies are based on the tight-binding Hamiltonian[11,14]

$$H = \sum_m \varepsilon_{mm} a_m^+ a_m + \sum_{m \neq n} V_{mn} a_m^+ a_n$$
$$+ \sum_\lambda \hbar\omega_\lambda (b_\lambda^+ b_\lambda + 1)$$
$$+ \sum_{m\lambda} g_{\lambda mm} \hbar\omega_\lambda (b_\lambda + b_{-\lambda}^+) a_m^+ a_m \qquad (2)$$
$$+ \sum_{m \neq n, \lambda} f_{\lambda mn} \hbar\omega_\lambda (b_\lambda + b_{-\lambda}^+) a_m^+ a_n$$

Here, the operators $a_m^+ (a_m)$ and $b_\lambda^+ (b_\lambda)$ represent, respectively, creation (annihilation) of an electron at site m with on-site energy ε_{mm} or a phonon belonging to mode λ with frequency ω_λ.

V_{mn} is the electronic transfer integral coupling two adjacent molecules m and n. $g_{\lambda mm}$ ($f_{\lambda mn}$) is the dimensionless coupling constant between phonon λ and the electronic term ε_{mm} (V_{mn}). The main difficulty for an accurate description of the charge transport mechanism in organic molecular semiconductors is that the relative magnitude of several factors in the Hamiltonian, i.e., V_{mn}, $\hbar\omega_\lambda$, $g_{\lambda mm}\hbar\omega_\lambda$, $f_{\lambda mn}\hbar\omega_\lambda$ and k_BT, is not well understood in real systems (k_B is the Boltzmann constant and T is the temperature).[11]

The temperature dependence of the mobility is widely studied as a means to better understand the charge transport mechanism in semiconducting materials.[9,14] Recent experimental evidence in naphthalene,[16] pentacene,[17] and ruberene[18] single crystals has shown that such intrinsic charge mobility generally decreases with temperature, following a power-law dependence: $\mu(T) \sim T^{-\alpha}$. Several models have been proposed to explain this aspect of the transport behavior. The first such attempt used the standard wide-band theory, which is used extensively

Xiaodi Yang was born in Henan, China, 1981. She obtained her PhD under the guidance of Professor Zhigang Shuai in 2008 from the Institute of Chemistry, Chinese Academy of Sciences. Her work focused on theoretical calculations of charge mobility in organic functional materials using the hopping description. She is currently a faculty member in the Laboratory of Advanced Materials, Fudan University, Shanghai.

Xiaodi Yang

Qian Peng was born in Henan, China, in 1978. She is a research assistant in Key Laboratory of Organic Solids, the Institute of Chemistry, CAS. She received her MS degree in 2004 on "theoretical studies on some small inorganic molecular and large complex compounds" from Northwest University, under the supervision of Prof. Zhenyi Wen, and her PhD in 2008 on "theoretical study on the process of excited states in isolated large organic molecules" from the Institute of Chemistry, CAS, under the supervision of Prof. Zhigang Shuai. Her research interests are molecular excited state dynamics and opto-electronic properties of organic materials.

Qian Peng

Qikai Li completed his undergraduate study in Physics at Zhongshang University, Guangzhou, in 1983, and obtained his PhD in Materials Physics and Chemistry at University of Sciences and Technology Beijing, Beijing in 2002. From 2002 to 2006 he was a postdoc in the Department of Materials Science and Engineering at Georgia Institute of Technology. He is now working at the Institute of Chemistry, Chinese Academy of Sciences. His interests are in computing materials science and parallel computing, self-assembly of organic materials, and solar cells.

Qikai Li

Zhigang Shuai received his PhD in 1989 from Fudan University, Shanghai. From 1990 to 2001, he worked in the University of Mons-Hainaut, Belgium, as a research scientist. From 2002, he became a professor at the Institute of Chemistry, CAS, in Beijing. Since May 2008, he is a full professor at the Department of Chemistry of Tsinghua University in Beijing. He is an elected member of the International Academy of Quantum Molecular Science (2008) and a Fellow of the Royal Society of Chemistry (2009). The major research interests in his group are theoretical modeling of organic functional opto-electronic materials and devices. He has authored or coauthored more than 200 research articles.

Zhigang Shuai

in inorganic materials.[19,20] In this model, the electron–phonon coupling is regarded as a perturbation and the charge is delocalized over the crystal. The carrier mobility decreases with temperature because of the increased scattering probability by phonons. The polaron model is also regarded as a candidate and has been extensively discussed in the literature.[10,21–24] Within this description, the electron is surrounded by phonon clouds, forming a quasi-particle (polaron) due to strong electron–phonon interaction. The power law dependence of mobility with temperature can be well obtained within this model as being due to the polaron bandwidth narrowing effect.[25] The hopping model, which assumes that the charge carriers are completely localized and diffuse by hopping from molecule to molecule, is often employed to describe disordered systems.[26] The hopping process is thermally activated since higher temperature provides more energy for charge carriers to overcome the energy barriers.[14] However, when nuclear tunneling effects, from the quantum nature of vibrations between localized molecular states are included, the experimentally-observed decrease in mobility with increasing temperature can be well reproduced.[27,28] Thus, the hopping mechanism can not be excluded based solely on the decrease of the carrier mobility with temperature, observed in polyacenes or rubrene.[29]

Unlike inorganic semiconductors, organic molecules are held together by weak van der Waals interactions. Therefore, several new characteristics are present in the charge transport mechanism. The intermolecular transfer integrals are usually small, on the order of a few tens of an meV.[25] Cheng et al. used a band model to investigate the transport properties for polyacenes, but found that the mean free path of charge carriers becomes shorter than the lattice constant at high temperatures, indicating the adequacy of a localized picture.[20] The weak intermolecular interactions in molecular systems also lead to enhanced molecular and lattice distortions from thermal motions. Since the intermolecular transfer integrals are largely related to the relative positions of adjacent molecules, the translational symmetry of the electronic Hamiltonian can be strongly purturbed by the resulting strong thermal fluctuations in transfer integrals.[30] After considering these fluctuations, the charge carriers are found to be localized, even in pentacene, which is known to have a low reorganization energy and large intermolecular electronic coupling.[31] Based on the above evidence, a localized charge hopping picture is more appropriate to describe most organic molecular materials, especially near room temperature. Due to the fact that the room-temperature mobility is mostly important for real applications, the hopping description of charge transport based on the localized picture has gained increasing attention in the literature as a means to explain the experimental data and to generate molecular design strategies for semiconducting materials.[28,32–40]

In this tutorial review, we describe how to calculate the charge mobility in organic molecular semiconductors with modern quantum chemistry tools. Section 2 describes quantum chemical approaches to compute the molecular parameters that govern the intermolecular charge transfer process, such as reorganization energy and transfer integrals, followed by a description of the use of random walk numerical mesoscopic scale simulations to model charge diffusion based on these computed microscopic parameters. Some applications of this approach and molecular design strategies for obtaining high mobility materials are outlined in Section 3. Molecular materials cover a wide range of microscopic parameters. Regarding the relative magnitude of intermolecular charge transfer rate with respect to the reorganization energy, Section 4 discusses recent attempts to go beyond the semiclassical Marcus theory by considering nuclear tunneling effects and non-perturbative effects. A summary and outlook are presented in the last section.

2. Computational methodologies

Within the hopping description, the charge transport can be characterized by a diffusion process, in which the charge carrier hops between adjacent molecules according to the charge transfer rates that apply in the absence of an external electric field. In the low field limit, the carrier mobility (eqn (1)) can be well described by the Einstein relation:

$$\mu = eD/k_{B}T \qquad (3)$$

where e is the electron charge and D is the charge diffusion coefficient. For a n-dimensional system, D is defined as the ratio between the mean-square displacement and the diffusion time:[41]

$$D = \frac{1}{2n}\lim_{t\to\infty}\frac{\langle r^2\rangle}{t} \qquad (4)$$

For a spatially isotropic system, the homogeneous diffusion constant D can be approximately evaluated by:[35]

$$D = \frac{1}{2n}\sum_{\alpha} r_{\alpha}^2 k_{\alpha} p_{\alpha} \qquad (5)$$

where α runs over all nearest adjacent molecules and r_{α}, k_{α} and p_{α} are the corresponding center-to-center hopping distance, charge transfer (CT) rate, and hopping probability ($p_{\alpha} = k_{\alpha}/\sum_{\beta}k_{\beta}$), respectively. Eqn (5) is valid when the CT rates k are close to each other. In addition, when considering only one neighbor, the diffusion constant along a single molecular dimer is simply defined as:[38]

$$D = \frac{1}{2}kr^2 \qquad (6)$$

where k and r are the charge transfer rate and intermolecular distance for the dimer. These simplified formulas are widely used in the literature to give qualitative insights into the charge transport properties.[32,33,35–38]

2.1 Charge diffusion through numerical random walk simulation

The intermolecular charge transfer rate between different dimers in organic materials can differ by orders of magnitudes. Futher, in thin film phases, grain boundaries are present. Such inhomogeneities indicate the inadequacy of either eqn (5) or (6) to describe actual materials. A random walk approach can instead be performed to simulate the diffusion process of the charge carrier in the presence of such inhomogeneities.[28,34,40] Within this approach, an arbitrary site (molecule) within the bulk is initially chosen as the starting position for the charge. The charge then has a probability of p_{α} to hop to the αth
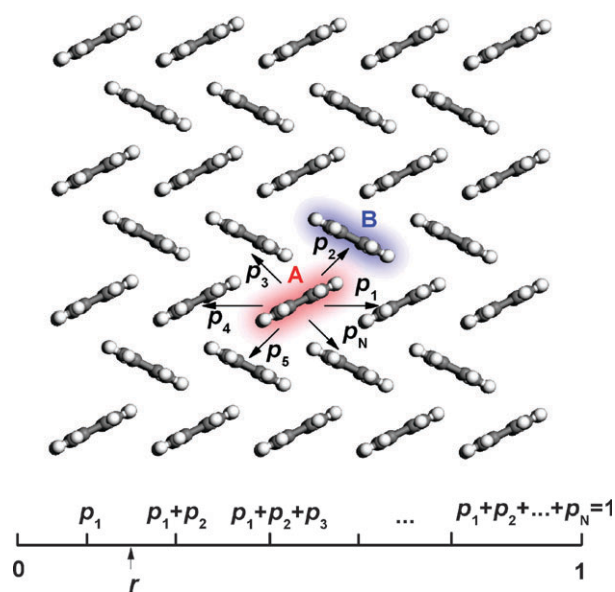
Fig. 1 (Top) Schematic representation of the charge hopping pathways from molecule A to its neighbors (N of them) with the probability $p_1, p_2, \ldots,$ and p_N. (Bottom) A unit length is divided into N parts according to each probability. A uniformly distributed random number (r) decides which path is chosen for charge hopping $e.g.$, to molecule B if $p_1 < r < p_1 + p_2$. Thereby, the larger p_2 is, the more probable it is for the charge to go to B.

Fig. 2 A typical evolution of the square displacement of ten individual simulations and the mean-square displacement over two thousand simulations. Reprinted with permission from ref. 39.

neighbor. In practice, in order to determine the next site of the charge in a statistical sense, a random number r uniformly distributed between 0 and 1 is generated. If $\sum_{\beta=1}^{\alpha-1} p_\beta < r < \sum_{\beta=1}^{\alpha} p_\beta$, the charge hops to the αth neighbor with a hopping time $1/k_\alpha$ (Fig. 1), which assumes no correlation between the hopping events along different paths. The simulation continues until the diffusion distance exceeds the lattice constant by at least 2–3 orders of magnitude. This process is repeated thousands of times and averaged to get a linear relationship between mean-square displacement and simulation time. A typical evolution of the mean-square displacement is shown in Fig. 2. From the resulting diffusion coefficient (eqn (4)), the mobility is finally evaluated by the Einstein formula (eqn (3)). Since, an electric field has not been applied in the simulation, the averaged displacement should be zero. For instance, different simulations will, after 1 or 2 ns, find different spatial locations for the final position of the charge. However, thousands of simulations will lead to ending points that uniformly surround the starting point (Fig. 3(a)). Thus, there should be no electric current, as expected in the absence of a field. Once an electric field is applied, the center of these ending points shifts uniformly as the simulation time increases. Taking a two-dimensional herringbone pentacene layer as an example, we show in Fig. 3 the ending points of 5000 simulations after 1 and 2 ns, as well as the calculated mobility without and with an applied electric field. It is seen that in the weak field limit, the two approaches give results that are in agreement. The field effect was incorporated in the driving force in the charge transfer process. The mobility increases with the field strength for small fields. Once the driving force
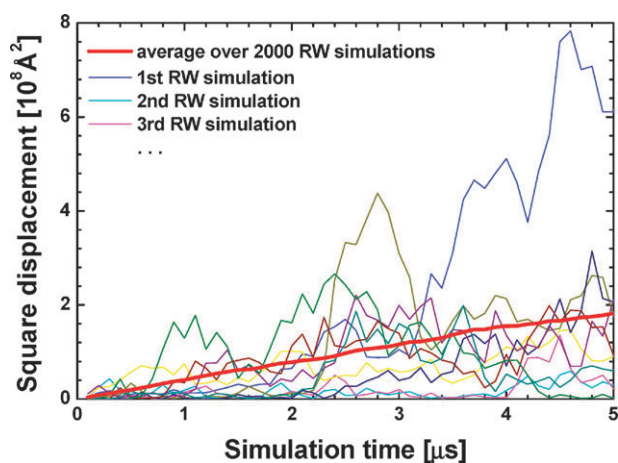
for the closest dimer becomes greater than the reorganization energy, the mobility starts to decrease with the field.

Due to the stochastic feature of the random walk simulation, the statistical error should be evaluated for the calculated mobility. Instead of running thousands of simulations again and again, a simpler approach is proposed.[28,34,40] If the number of individual simulation runs is sufficiently large, say two thousand, one can randomly select subsets of these runs and then compare the mobility, μ_i, obtained from each these subsets, where i indicates different subsets. The error of the calculated mobility can be estimated as $(\max\{\mu_i\} - \{\mu_i\})/2$. Normally, 2000 simulations can achieve an error within 5% which is already too small to influence the numerical conclusions.[28,34]

2.2 Marcus charge transfer theory

The charge transfer rates between molecular dimers are needed as inputs to the above random walk simulations. Since the widely studied molecular semiconductors contain only one kind of molecule, the charge transfer in an adjacent molecular dimer, M_1 and M_2, is a self-exchange reaction process. The initial and final states can be represented as $(M_1{}^+ M_2\rangle$ and $(M_1 M_2{}^+\rangle$, respectively, with M^+ denoting the charge on molecule M.

The widely used charge transfer rate from the classical Marcus theory reads:[42]

$$k = \frac{V^2}{\hbar}\sqrt{\frac{\pi}{\lambda k_B T}}\exp\left(-\frac{(\lambda + \Delta G^0)^2}{4\lambda k_B T}\right) \qquad (7)$$

Here V is the transfer integral between the initial and final states, λ is the reorganization energy which is defined as the energy change associated with the geometry relaxation during the charge transfer, and ΔG^0 is the relevant change of total Gibbs free energy. In the self-exchange reaction, ΔG^0 equals zero and eqn (7) then becomes

$$k = \frac{V^2}{\hbar}\sqrt{\frac{\pi}{\lambda k_B T}}\exp\left(-\frac{\lambda}{4 k_B T}\right) \qquad (8)$$

The charge transport is therefore modeled as a thermal activation process over a barrier of $\lambda/4$.
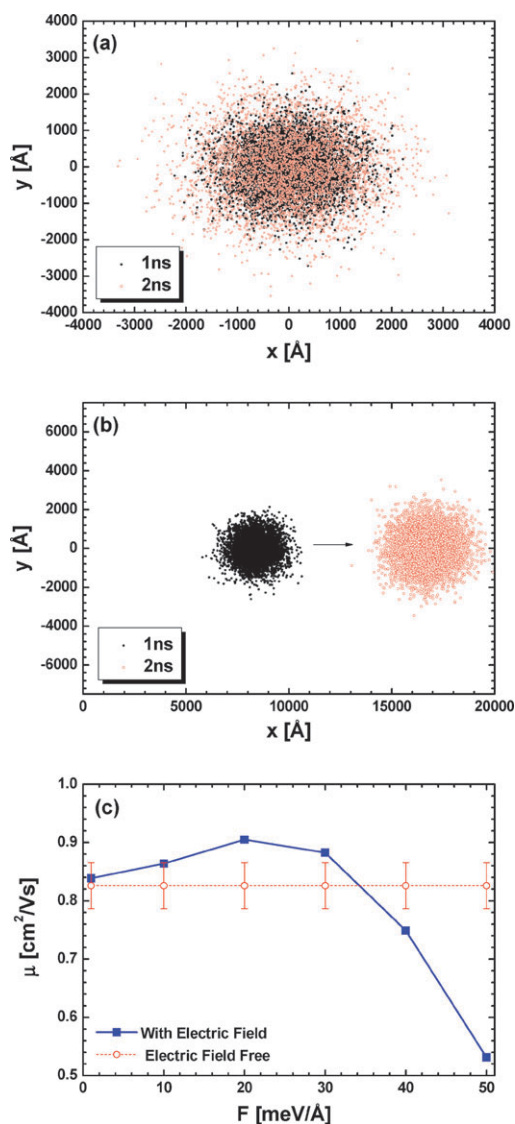
Fig. 3 Field effect on the charge diffusion obtained from 5000 simulations: (a) field-free diffusion; (b) charge diffusion at an electric field along the x-axis ($F = 10^5$ V cm^{-1}) after 1 ns (black dots) and 2 ns (red dots); (c) field-dependent mobility.

2.3 Reorganization energy and transfer integral

From eqn (8), it is clear that there are two key factors influencing the charge transfer rate: the reorganization energy and the transfer integral. A number of papers have described how to calculate these parameters from first-principles.[13,14,40]

The reorganization energy has both internal and the external contributions, with the internal contribution arising from changes in the geometry of the molecular dimer when the electron transfer takes place, and the external contribution arising from changes in the surrounding media that accompany the charge transfer. At this stage, the external part is often neglected and only the internal contribution is taken into account in organic crystals, in contrast to the case of charge transfer in solution where the external part dominates.[14,32–38] The internal part is a sum of two relaxation energy terms: (i) the energy difference of the neutral molecule in the optimal
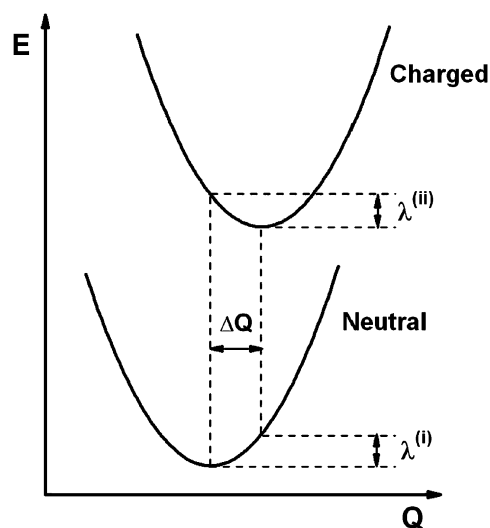
Fig. 4 Schematic representation of the potential energy surfaces of the neutral and charged molecules with respect to the reaction coordinate. The sum of the two relaxation energies $\lambda^{(i)}$ and $\lambda^{(ii)}$ is the internal reorganization energy.

charged geometry and in the equilibrium neutral geometry, $\lambda^{(i)}$, and (ii) the energy difference of the charged molecule in these two geometries, $\lambda^{(ii)}$, as sketched in Fig. 4. The reorganization energies for hole transport (λ^+) and electron transport (λ^-) are calculated from positively and negatively charged molecules, respectively.

Several methods have been proposed to evaluate the transfer integral within a molecular dimer. The simplest way is the frontier orbital energy level splitting method,[43] in which the transfer integral between identical molecular orbitals in the two isolated molecules corresponds to half of their energy level splitting when they form a dimer. More strictly, the splitting should be taken at the transition state point during the charge transfer reaction.[44] In fact, the simple energy level splitting method should be used with caution because the splitting is equal to $\sqrt{(e_1 - e_2)^2 + 4V^2}$, where e_1 (e_2) is the on-site energy of molecule 1 (2) and V is the true transfer integral.[45] If two identical molecules are not in equivalent positions in the crystal, they possess different site-energies due to the different environments. For instance, in a typical herringbone structure, the frontier orbital splitting of either the highest occupied molecular orbital (HOMO) or the lowest unoccupied molecular orbital (LUMO), can be found to be maximized for a tilt angle of 90°,[43] while the transfer integral is almost zero after considering the site-energy difference.[45] Thus considering only the energy level splittings could lead to a conceptually wrong materials design strategy.

A more direct and simpler way to calculate the transfer integral involves direct evaluation of the coupling element between frontier orbitals using the unperturbed density matrix of the dimer Fock operator.[46] In this case, the transfer integral within a molecular dimer, V_{12}, reads:

$$V_{12} = \langle \psi_1 | F | \psi_2 \rangle \qquad (9)$$

where ψ_1 and ψ_2 are the frontier orbitals of the two isolated molecules 1 and 2 in the dimer. $F = SC\varepsilon C^{-1}$ is the Fock
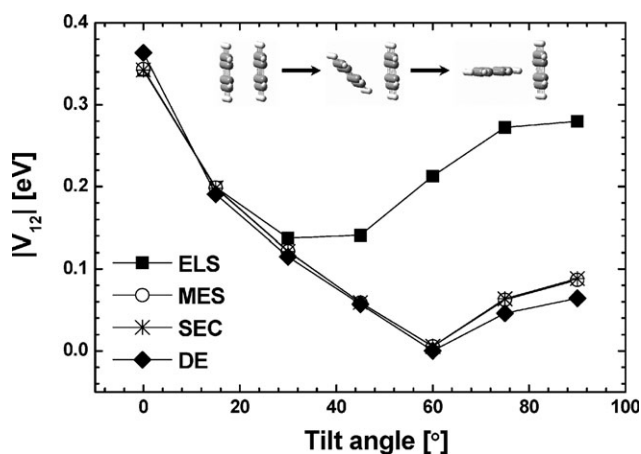
Fig. 5 Evolution of the hole transfer integral for pentacene dimer as a function of the tilt angle θ. The distance between the two molecules is $R = (3.5 + 1.5\sin\theta)$ Å. The results of all four methods, *i.e.*, ELS (energy level splitting),[43] MES (minimized energy splitting along reaction path),[44] SEC (site-energy correction),[45] and DE (direct evaluation),[46] are compared. Reprinted with permission from ref. 40.

operator, where S is the overlap matrix, and C and ε represents the Kohn–Sham orbital coefficients and energies obtained from one-step diagonalization without interaction, which can be performed in the Gaussian 03 package.[47] Since there is no need to construct the dimer Hamiltonian or to obtain the energy levels, this direct evaluation method has much less computational cost than other methods.

As shown in Fig. 5, the above four methods are compared for the pentacene dimers with different tilt angles from cofacial to perpendicular. It is seen that for the cofacially packed dimer, the four methods give almost identical values. However, the energy level splitting method begins to deviate from the other methods as the tilt angle is increased. The other three methods remain nearly identical, especially when the tilt angle is smaller than $60°$.[40]

3. Molecular design strategy for high mobility materials

For a given material, the charge mobility can now be predicted from computation, but only within the hopping description and only provided detailed information is available about the molecular packing. The reorganization energy and the transfer integrals are first obtained based on the single molecule and the molecular dimers, respectively. Based on these factors, the charge transfer rates between all adjacent molecules can be evaluated, as well as the diffusion constant and ultimately the charge mobility.

According to the Marcus rate formula (eqn (8)), small internal reorganization energy and large intermolecular transfer integrals are helpful to speed up the charge transfer processes between neighboring molecules. The random-walk simulation indicates that smoothly distributed charge transfer channels in the network are favorable to the global charge mobility. The application of these computational methods on typical organic molecular semiconductors, as shown in Fig. 6,
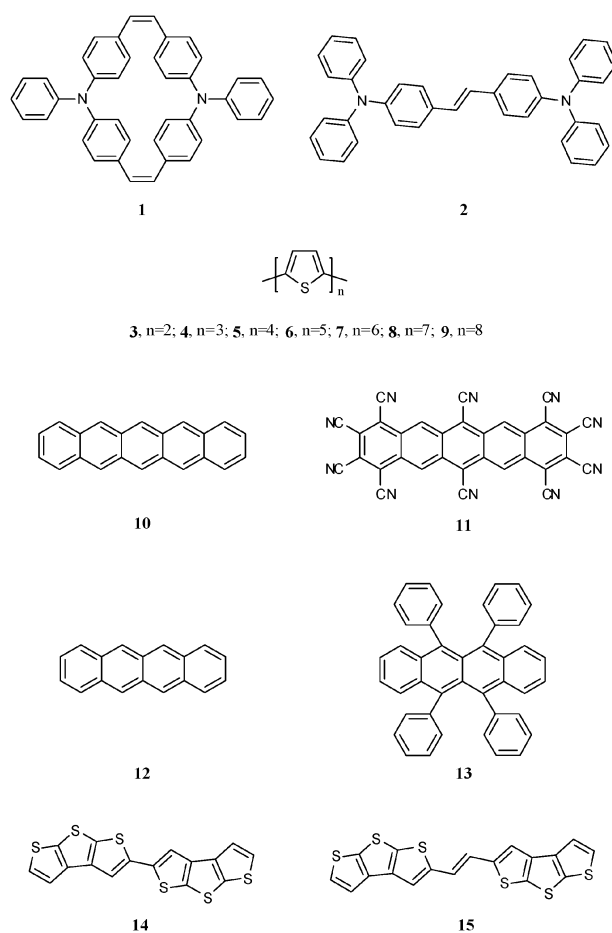
Fig. 6 Chemical structures of the compounds discussed here.

can provide real guidance for designing materials with high carrier mobility.

3.1 Toward reducing the internal reorganization energy

The internal reorganization energy originates from molecular deformations upon charging. Since these are related to intramolecular degrees of freedom, rigid molecules should have smaller values than flexible molecules. Density functional theory was applied to calculate the molecular reorganization energies for compounds **1–11**, which are depicted in Table 1. As a first example for molecular design, we take a look at triphenylamine, which is a classical hole transport material. To further improve the transport property, one can construct dimeric or higher configurations, for instance, in the form of a macrocycle (**1**, Fig. 6) or in a linear chain (**2**, Fig. 6).[32] Intuitively, chains should be more conductive. Quantum chemistry calculations found that λ^+ of compound **1** (173 meV) is much smaller than λ^+ of compound **2** (317 meV).[33] The difference arises from the difference in geometry relaxation on going from neutral to cation equilibrium forms.[33] It is found that the rotation of the phenyl groups is restricted in **1** while large relaxation of the biphenyl core is observed in **2**. Since the transfer integrals are found to be very close for **1** and **2**, the room-temperature hole mobility for **2** based on eqn (5) is calculated to be 1.9×10^{-3} cm^2 V^{-1} s^{-1}, which is one order of magnitude smaller than that of **1**, 2.7×10^{-2} cm^2 V^{-1} s^{-1},

Table 1 Internal reorganization energies of compounds **1–11** for hole and electron by adiabatic potential (AP) surfaces of the neutral and cation species and by normal mode (NM) analysis in meV. Calculations are performed in Gaussian 03 package at the B3LYP/6-31G* level for compounds **1–9**, and at the B3LYP/6-31 + G* level for **10** and **11**[47]

Compound	λ^+ (AP)	λ^+ (NM)	λ^- (AP)
1[a]	173	—	—
2[a]	317	—	—
3[b]	361	364	—
4[b]	316	323	—
5[b]	286	288	—
6[b]	265	274	—
7[b]	244	255	—
8[b]	224	238	—
9[b]	203	212	—
10[c]	94	—	133
11[c]	75	—	87

[a] Ref. 33. [b] Ref. 34. [c] Ref. 38.

mainly due to the difference in reorganization energy.[33] These values compare well with the best experimental results of 1.5×10^{-2} and 2×10^{-4} cm^2 V^{-1} s^{-1} for **1** and **2**, respectively.[32]

One of the advantages of organic materials is their ability to form series of oligomers with similar chemical structures but different chain lengths, such as the oligothiophenes (nT) (**3–9**, Fig. 6). It is found that λ^+ monotonously decreases with the number of thiophene rings from about 360 meV for 2T to 210 meV for 8T (Table 1).[14,34] This trend is also observed in other systems, *e.g.*, oligoacenes,[35] oligothienoacenes,[36] and various families of oligoheterocycles.[37] Hutchison and co-authors argued that the positive charge becomes more delocalized in

longer conjugated oligomers, therefore the internal reorganization energy gets smaller due to less geometric distortion accompanying the charge transfer.[37]

Substituent effects are of primary interest in molecular design. Although several functional groups (–F, –OR, –CF$_3$, and –NH$_2$) tend to increase the internal reorganization energy compared with their parent compounds, cyanation has a significant opposite trend.[37] Recently, Chao and co-authors found that cyanation can strongly reduce both λ^+ and λ^- for pentacene (**10**, Fig. 6),[38] one of the most promising hole transport materials.[48] One cyanated pentacene derivative, compound **11** (Fig. 6), has a λ^+ of 75 meV and λ^- of 87 meV, compared with the 94 meV and 133 meV for pentacene (Table 1). The nonbonding character of the cyano groups are found to further extend the electron delocalization, and thus lead to a smaller reorganization energy.[37,38]

3.2 Toward increasing the intermolecular transfer integrals

Unlike the reorganization energy, the transfer integrals are strongly related to the intermolecular interaction, which requires going beyond single molecular properties. Brédas *et al.* have systematically studied the evolution of the transfer integral with respect to the intermolecular displacement and orientation for a variety of organic compounds.[13,49–52] The results indicate that large variations in the transfer integrals can arise from small distortions in the intermolecular geometry. This poses significant challenges for computations of transfer integrals in systems for which the exact molecular packing is not yet known. However, it also brings promising opportunities to molecular design since either functionalizing the molecular
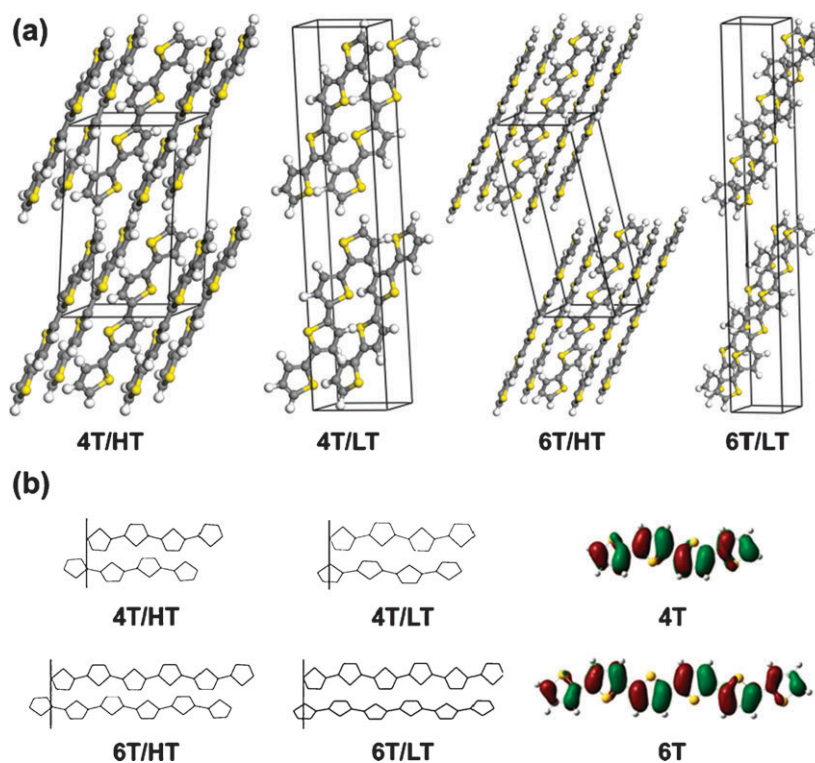
Fig. 7 (a) Crystal structures of 4T/HT, 4T/LT, 6T/HT and 6T/LT. (b) Intermolecular displacements taken from the crystal packing along the long axis of thiophenes for the dominant pathway and HOMOs of 4T and 6T. Reprinted with permission from ref. 34.

structure or changing the environmental condition may modify the intermolecular positions in a manner that increases the intermolecular electron coupling.

Extensive studies have been made on the functionalization of acenes, especially tetracene (**12**, Fig. 6) and pentacene (**10**, Fig. 6).[53,54] The most successful example is undoubtedly rubrene (**13**, Fig. 6), which is a tetraphenyl derivative of tetracene. The phenyl substitution improves the molecular packing in rubrene, and the largest intermolecular transfer integral increases from 71 meV for tetracene to 102 meV for rubrene due to an advantageous intermolecular lateral displacement.[28] Although the reorganization energy of rubrene is larger than tetracene (150 meV *vs.* 105 meV), the calculated hole mobility for rubrene (2.39 cm^2 V^{-1} s^{-1}) is much larger than that of tetracene (0.67 cm^2 V^{-1} s^{-1}), a trend that agrees well with experiment.[8] Similar situations can also be found in pentacene derivatives. With the available crystal structures, transfer integrals up to 170 meV has been found and mobilities as high as 35 cm^2 V^{-1} s^{-1} have been predicted based on enhanced intermolecular transfer integrals.[38]

Molecular materials may have several polymorphs in the crystal form. For instance, 4T (**5**, Fig. 6) and 6T (**7**, Fig. 6) form typically two polymorphs, namely the high-temperature (HT) phase and the low-temperature (LT) phase, depending on the sublimation temperatures.[55–58] A distinct difference lies in the number of molecules in the unit cell: the HT phase has two, while the LT phase has four (Fig. 7(a)). The slight difference in the crystal packing results in very different transfer integrals, *e.g.*, the largest term is 40 meV for 4T/HT and 36 meV for 6T/HT, which are about twice the magnitude of the largest term for 4T/LT and for the HT, 18 meV.[34] Focusing on the intermolecular displacements of these dominant dimers, it is found that there exists a displacement of about half a thiophene ring width for the LT phase, while for the HT phase, the displaced length is about one thiophene ring (Fig. 7(b)). Since the sign of the HOMO orbitals has a period of half a thiophene ring, the different displacements in HT and LT phases result in significantly different intermolecular coupling strengths. As a result, the calculated hole mobility of the HT phase is about four times as large as the LT phase.[34] Along this line, Deng and Goddard III earlier proposed another packing structure of a pentacene polymorph (**10**, Fig. 6) with much larger intermolecular transfer integrals.[35] The predicted hole mobility was found to be 2.8 times larger than the value of the normal crystal.

3.3 Toward a better charge transport network

The efficiency of charge transport should be strongly related to the crystal packing, which may provide entirely different transport networks. Compounds **14** and **15** (Fig. 6) based on annelated β-trithiophenes, have distinctly different crystal packings: **14** has the sandwich-herringbone arrangement, while **15** stacks in the normal herringbone structure (Fig. 8). As for the intra-layer transfer integrals for hole transport, the values are rather uniform for **15**, ranging from 11.3 to 35.4 meV.[39] In contrast, the transfer integral of the isolated cofacial dimer in **14** (62.2 meV) is much larger than all the others (less than 7.4 meV). As a result, when tracking the trajectories from the numerical simulation for **14**, one finds that the hole spends a
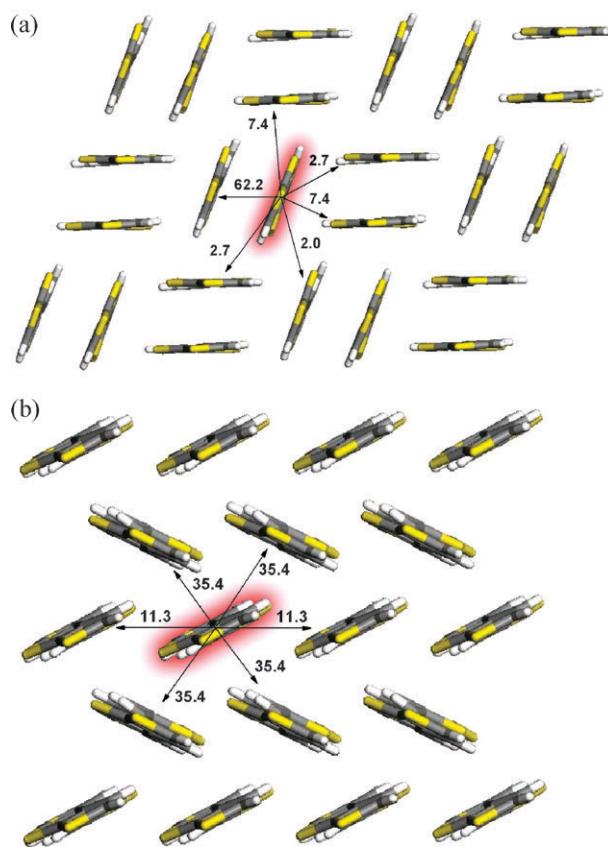
Fig. 8 Crystal packing of compounds (a) **14** and (b) **15**. The arrows indicate all the nearest intralayer neighbors of the molecule which is highlighted in red. The values are the corresponding transfer integrals in meV, which are calculated at the DFT-B3LYP/6-31G* level with the Gaussian 03 package.[47]

considerable proportion of time oscillating between the cofacial dimers and such oscillations do not contribute to the overall mobility. As a result, the charge is localized in the dimer, and it is difficult to move outside of the dimer and into the network. For **15**, due to the symmetric crystal structure, the probabilities for the charge transfer are similar in different directions, resulting in a smooth charge diffusion. The calculated hole mobility for **15** (0.072 cm^2 V^{-1} s^{-1}) is about 48 times as large as that for **14** (0.0015 cm^2 V^{-1} s^{-1}), agreeing well with experiment.[39] Note that such a trend is strongly related to the charge diffusion pathway structure. Therefore it can not be reproduced by eqn (5) or (6) due to its uniform diffusion assumption. Experimental studies show that tetrathiafulvalene derivatives can also form different crystal structures, *e.g.*, the sandwich-herringbone, face-to-face and herringbone configurations.[59] We note that there is a clear correlation between the measured mobility and the crystal packing.[59] Considering their similarity to trithiophene derivatives, such experimental observation is certainly related to the different charge transport networks.

4. Nuclear tunneling and non-perturbative effects in charge transfer

In the above studies, the classical Marcus theory is widely used to describe the charge transfer rates for room-temperature

430 | *Chem. Soc. Rev.*, 2010, **39**, 423–434

This journal is © The Royal Society of Chemistry 2010

charge transport properties. At lower temperature, or when higher frequency modes are coupled with the charge transfer process, nuclear tunneling effects should be considered. In addition, the Marcus charge transfer theory assumes weak coupling. The transfer integrals in organic crystals usually vary by several orders of magnitude,[25,34,39] which could go beyond the applicable range of first-order perturbation approaches. It is highly desirable to develop methods which can be applied from weak to strong coupling regimes.

4.1 Multimode quantum charge transfer rate

The quantum multimode expression for the charge transfer rate, under the displaced harmonic oscillator approximation, can be derived from the Fermi Golden Rule (FGR) as:[60]

$$k = \frac{|V|^2}{\hbar^2} \int_{-\infty}^{\infty} \mathrm{d}t$$

$$\times \exp\left\{ i\omega_{fi}t - \sum_j S_j[(2n_j + 1) - n_j e^{-i\omega_j t} - (n_j + 1)e^{i\omega_j t}] \right\} \tag{10}$$

Here, $\omega_{fi} = \Delta G^0/\hbar$ goes to zero, $n_j = 1/(\exp(\hbar\omega_j/k_B T) - 1)$ is the occupation number of the jth phonon mode with frequency ω_j, and S_j is the Huang–Rhys factor measuring the coupling strength between the charge carrier and the jth mode. Note that eqn (10) is a rather general expression. In the strong coupling ($\sum_j S_j \gg 1$) and high temperature ($\hbar\omega_j/k_B T \ll 1$) limits, where the short-time approximation can be applied, eqn (10) goes to the Marcus formula (eqn (7)), and the reorganization energy is related to the Huang–Rhys factors by $\lambda = \sum_j S_j \hbar\omega_j$.[28] Alternatively, when the high-frequency intramolecular modes are represented by a single effective mode and treated quantum-mechanically, while all the low-frequency intermolecular modes are treated classically, eqn (10) goes to the Bixon–Jortner formula for the charge transfer rate.[61]

The Huang–Rhys factor related to the ith vibration mode is calculated from a normal-mode analysis: $S_i = k_i \Delta Q_i^2/(2\hbar\omega_i)$, where ΔQ_i represents the projection of the rigid displacement between the neutral and charged equilibrium geometries onto the ith normal mode (Fig. 4), k_i is the corresponding force constant and ω_i is the circular frequency. This normal mode process also provides another way to calculate the total reorganization energy, from the Huang–Rhys factors: $\lambda = \sum_i \hbar\omega_i S_i$. We note that the result obtained from the normal-mode analysis and that obtained directly from the adiabatic potential-energy surfaces of neutral/charged molecules are very close in several cases (Table 1),[13,34] implying that the harmonic oscillator approximation is quite satisfactory. The normal mode analysis provides an insightful way to see how the total reorganization energy is distributed into the vibrational modes: $\lambda_i = \hbar\omega_i S_i$, which is important for understanding the coupling strength between charge and different phonons for a quantum theory treatment.

The nuclear tunneling effect on the charge transfer rate is investigated for the polyacenes and rubrene. In the case of tetracene (**12**, Fig. 6), taking the dimer with the largest transfer integral as an example, the hole transfer rate as a function of
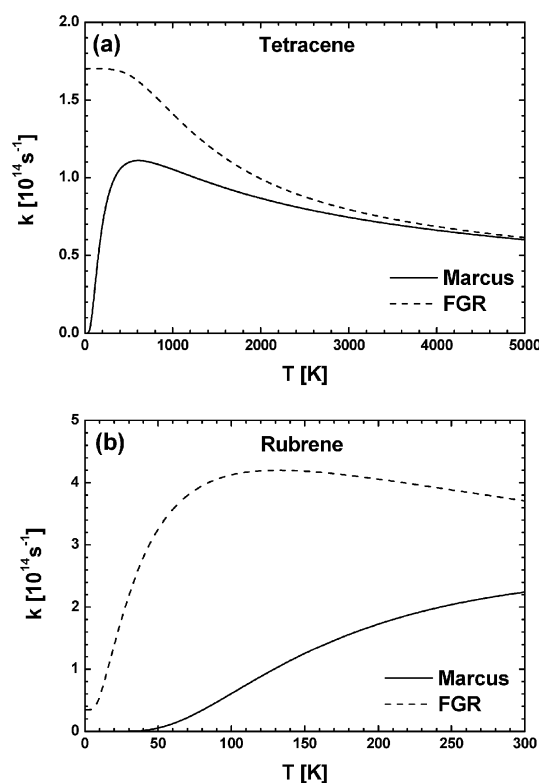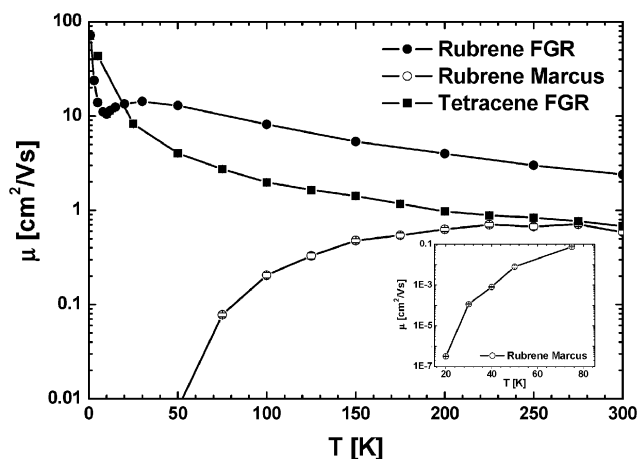

Fig. 9 Hole transfer rates from Marcus theory and FGR as a function of temperature for the dimer with the largest transfer integral in (a) tetracene and (b) rubrene. Reprinted with permission from ref. 28.

temperature is depicted in Fig. 9(a).[28] The Marcus rate increases exponentially from zero at low temperature to reach a maximum, which is related to the reorganization energy, and then levels off and decreases at higher temperatures, showing a thermally activated behavior as mentioned in section 2. When nuclear tunneling effects are included, the FGR rate remains constant at low temperature and then decreases because of nuclear scattering. At high temperature, the FGR rate tends towards coincidence with the Marcus curve. For rubrene (**13**, Fig. 6), the behavior of the Marcus rate is the same as that of tetracene, while the FGR result is quite different: the rate has a very short plateau at sufficiently low temperature, and then rises before it starts to level off and decrease (see Fig. 9(b)). Detailed analysis of the Huang–Rhys factors for all normal modes shows that there is a large contribution to rubrene from the low-frequency region (about 20 cm^{-1}), due to the twisting motions of the four phenyl groups, which notably differs from tetracene.[28] These extremely low frequency modes can be well approximated classically even at very low temperatures, behaving as Marcus-like thermal activation, and are responsible for the enhanced charge transfer rate.

The random walk simulation results for the hole mobilities of tetracene and rubrene as a function of temperature are shown in Fig. 10. The transport by Marcus rate is of thermal activation type, while the FGR gives an overall "bandlike" behavior (decreasing with temperature), except that there are some fine features at low temperature for rubrene. The mobility decreases rapidly from 1 to 10 K, increases slowly with

Fig. 10 Hole mobilities as a function of temperature in rubrene and tetracene using Marcus and FGR charge transfer rates. The inset shows the mobility from Marcus theory at low temperatures. Reprinted with permission from ref. 28.

Fig. 11 Arrhenius plots of the charge transfer rates in quaterthiophene for two dimers with transfer integrals of (a) 4 meV and (b) 40 meV. The results of GNTST (open squares), FGR (solid line) and Marcus (dashed line) theories are shown. Reprinted with permission from ref. 40.

temperature up to 30 K, and then decreases again at higher temperatures, coinciding with the behavior of the hole transfer rate at this temperature region. Note that such a temperature dependence of mobility is often regarded as the band-hopping transition which was first observed in naphthalene single crystals,[62] and has been successfully explained within small polaron theories.[22–24] After inclusion of the nuclear tunneling effect, the hopping description is also able to reproduce this kind of transition as well as the pure bandlike behavior, as seen in Fig. 10.

4.2 Generalized nonadiabatic transition state theory: non-perturbative effects

Both Marcus theory and FGR are based on a first order perturbative treatment of the intermolecular electronic coupling. The generalized nonadiabatic transition state theory (GNTST) has been shown to be applicable from the weak to strong coupling regimes.[40] Within the limit of weak coupling, GNTST goes to FGR; and FGR goes to the Marcus theory at high temperatures.[40] It was derived from the rigorous flux-side correlation function[63] coupled with the Zhu–Nakamura nonadiabatic transition probability.[64] The GNTST charge transfer rate reads:[65]

$$k = Z_{mod}\sqrt{\frac{k_B T}{2\pi}} R_1 R_2 \qquad (11)$$

Here Z_{mod} represents the quantum mechanical correction of the partition function, R_1 corresponds to the ratio of the free energy on the seam surface and reactant partition function, and R_2 is the average nonadiabatic transition probability at the seam surface. The definitions of these parameters are explicitly given in ref. 65, and can be calculated with a simplified adaptive umbrella sampling approach combined with the histogram technique.[66]

The above theory has been applied to quaterthiophene (**5**, Fig. 6) and sexithiophene (**7**, Fig. 6), in close comparison with the Marcus and FGR methods.[40] For quaterthiophene, the temperature dependence of the hole transfer rate is shown in Fig. 11 with different transfer integrals: 4 and 40 meV. As
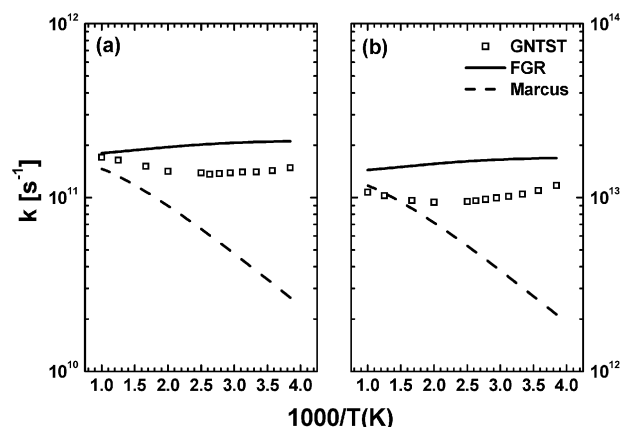
expected, all three methods tend to converge at high temperature when the transfer integral is as small as 4 meV. Also, the GNTST result is closer to FGR at low temperatures, at which Marcus theory fails due to the enhanced nuclear tunneling effect. More importantly, the FGR result is found to deviate from GNTST when the transfer integral increases to 40 meV.

5. Summary and perspectives

This tutorial review outlines a first-principles computational scheme based on the hopping description of charge mobilities. This approach can well describe the room-temperature mobilities in organic molecular semiconductors, and attain both qualitative and quantitative agreement with experiments. Several molecular design strategies for high mobility materials have been outlined from the points of view of molecular reorganization energy, intermolecular electronic coupling and the charge transport network. Computations indicate that rigid structures with extended conjugation, as well as substitutions such as cyanation, favor small reorganization energy. Modifying the molecular structure or changing the environmental conditions to favor different crystal phases can change the intermolecular bonding (anti-bonding) interactions and result in larger intermolecular transfer integrals. For an efficient charge transfer network, uniformly distributed intermolecular charge transfer is necessary. At a more fundamental level, we review the recent efforts in implementing more elaborate charge transfer theories that include nuclear tunneling and non-perturbative effects.

It should be noted that in organic molecular systems, thermal fluctuations in the molecular orientations may be strong, which could result in large fluctuations in intermolecular transfer integrals,[30] a fact that has not received much attention in the past. It has been argued that such dynamic disorder is the origin of the "band-like" behavior from a study for one-dimensional Su–Schrieffer–Heeger model.[31] The validity of such an argument for realistic higher dimensional systems deserves further investigation. Our preliminary work on a pentacene two-dimensional array shows that, although dynamic disorder does strongly hinder

the charge transport in one-dimensional molecular stacking chains, it has no significant influence for the two-dimensional case, within the charge hopping model containing nuclear tunneling effects.[67]

The molecular crystal structure is indispensable to computational predictions of the intrinsic charge mobility. This structure is taken from experimental measurement, making computations impractical for new molecules where there is no knowledge of the crystal packing structure. Therefore, it is highly desirable to develop computational methods to predict the crystal structure starting from the molecular structure. Since the intermolecular interaction is of weak character, predicting molecular crystal structure is one of the great challenges for computational chemistry. We notice that significant progress has been made in this direction recently.[68]

We also note that the present hopping description relies on the rate assumption, i.e., the charge population decays exponentially. When the rate process does not exist for the charge transfer within a single molecular dimer (e.g., due to very large transfer integrals) or when the time scale of the thermal fluctuations of onsite energies and transfer integrals are less than the transfer time within the dimer, the non-equilibrium nature of the reaction process should be included. Along this line, the time-dependent quantum methods for charge transfer can be considered, e.g., the linearized semi-classical initial value representation (LSC-IVR),[69] multi-configuration time-dependent Hartree (MCTDH) method,[70] path integral method,[71] and equation of motion for the reduced density matrix based on the Redfield theory.[72] Applying these methods to describe charge transfer phenomena in organic semiconductors deserves further explorations.

Going beyond the localized charge transport description is still of great theoretical interest. A first-principles projected Holstein–Peierls model has been found to qualitatively describe the contributions of intermolecular vs. intramolecular optical phonon vibrational modes,[22] as well as pressure and temperature effects.[23,24] However, the charge mobility is calculated to be one to two orders of magnitude larger than that of the single-crystal experimental measurements. Here, the acoustic phonon scattering has been ignored due to computational limitations: for acoustic phonons, one needs to deal with a supercell consisting of many unit cell, and for organic crystals, the large size of the unit cell already makes computations difficult. Thus, combining both optical and acoustic phonon scattering mechanisms remains a great challenge to development of a better description within a delocalized electron picture. A constant time approximation, based on a tight-binding band model with inclusion of electron–phonon scattering, indicates contradictory results when compared with experiment. Namely, assuming a delocalized band model results in a mean free path as short as the intermolecular distance.[20] Recent advancements in quantum dynamics simulations, which solve the time-dependent Schrödinger equation, can capture the essence of charge transport in electron–phonon interacting systems and so are promising for obtaining quantitative descriptions of both the temperature dependence and the absolute magnitude of the charge mobility for organic materials.[15] However, due to the expensive computational cost, current studies are limited to one-dimensional molecular arrays with very few phonon modes.[31,73] Thus, we recommend that these models should be further developed and studied, in comparison with the hopping description, to meet the demands of molecular design in organic electronics.

Acknowledgements

References

1 Y. Shirota and H. Kageyama, Chem. Rev., 2007, **107**, 953–1010.
2 A. R. Murphy and J. M. J. Fréchet, Chem. Rev., 2007, **107**, 1066–1096.
3 A. P. Kulkarni, C. J. Tonzola, A. Babel and S. A. Jenekhe, Chem. Mater., 2004, **16**, 4556–4573.
4 J.-M. Nunzi, C. R. Phys., 2002, **3**, 523–542.
5 R. A. Logan and A. J. Peters, J. Appl. Phys., 1960, **31**, 122–124.
6 T. Dürkop, S. A. Getty, E. Cobas and M. S. Fuhrer, Nano Lett., 2004, **4**, 35–39.
7 T. Tsumura, H. Koezuka and T. Ando, Appl. Phys. Lett., 1986, **49**, 1210–1212.
8 C. Reese and Z. N. Bao, Mater. Today, 2007, **10**, 20–27.
9 M. E. Gershenson, V. Podzorov and A. F. Morpurgo, Rev. Mod. Phys., 2006, **78**, 973–989.
10 T. Holstein, Ann. Phys., 1959, **8**, 343–389.
11 M. Pope and C. E. Swenberg, Electronic Processes in Organic Crystals, Oxford University Press, New York, 1982.
12 E. A. Silinsh and V. Čápek, Organic Molecular Crystals: Interaction, Localization, and Transport Phenomena, American Institute of Physics, New York, 1994.
13 J.-L. Brédas, D. Beljonne, V. Coropceanu and J. Cornil, Chem. Rev., 2004, **104**, 4971–5003.
14 V. Coropceanu, J. Cornil, D. A. da Silva Filho, Y. Olivier, R. Silbey and J.-L. Brédas, Chem. Rev., 2007, **107**, 926–952.
15 D. L. Cheung and A. Troisi, Phys. Chem. Chem. Phys., 2008, **10**, 5941–5952.
16 N. Karl, Synth. Met., 2003, **133–134**, 649–657.
17 O. D. Jurchescu, J. Baas and T. T. M. Palstra, Appl. Phys. Lett., 2004, **84**, 3061–3063.
18 V. Podzorov, E. Menard, J. A. Rogers and M. E. Gershenson, Phys. Rev. Lett., 2005, **95**, 226601.
19 W. Warta and N. Karl, Phys. Rev. B: Condens. Matter Mater. Phys., 1985, **32**, 1172–1182.
20 Y. C. Cheng, R. J. Silbey, D. A. da Silva Filho, J. P. Calbert, J. Cornil and J.-L. Brédas, J. Chem. Phys., 2003, **118**, 3764–3774.
21 K. Hannewald and P. A. Bobbert, Phys. Rev. B: Condens. Matter Mater. Phys., 2004, **69**, 075212.
22 L. J. Wang, Q. Peng, Q. K. Li and Z. Shuai, J. Chem. Phys., 2007, **127**, 044506.
23 L. J. Wang, Q. K. Li and Z. Shuai, J. Chem. Phys., 2008, **128**, 194706.
24 L. J. Wang, Q. K. Li and Z. Shuai, J. Mol. Sci. (Chinese), 2008, **24**, 133–138.
25 K. Hannewald, V. M. Stojanović, J. M. T. Schellekens, P. A. Bobbert, G. Kresse and J. Hafner, Phys. Rev. B: Condens. Matter Mater. Phys., 2004, **69**, 075211.
26 H. Bässler, Phys. Status Solidi B, 1993, **175**, 15–56.
27 D. D. Eley, H. Inokuchi and M. R. Willis, Discuss. Faraday Soc., 1959, **28**, 54–63.
28 G. J. Nan, X. D. Yang, L. J. Wang, Z. Shuai and Y. Zhao, Phys. Rev. B: Condens. Matter Mater. Phys., 2009, **79**, 115203.

29 R. M. Glaeser and R. S. Berry, *J. Chem. Phys.*, 1966, **44**, 3797–3810.
30 A. Troisi and G. Orlandi, *J. Phys. Chem. A*, 2006, **110**, 4065–4070.
31 A. Troisi and G. Orlandi, *Phys. Rev. Lett.*, 2006, **96**, 086601.
32 Y. B. Song, C. A. Di, X. D. Yang, S. P. Li, W. Xu, Y. Q. Liu, L. M. Yang, Z. Shuai, D. Q. Zhang and D. B. Zhu, *J. Am. Chem. Soc.*, 2006, **128**, 15940–15941.
33 X. D. Yang, Q. K. Li and Z. Shuai, *Nanotechnology*, 2007, **18**, 424029.
34 X. D. Yang, L. J. Wang, C. L. Wang, W. Long and Z. Shuai, *Chem. Mater.*, 2008, **20**, 3205–3211.
35 W. Q. Deng and W. A. Goddard III, *J. Phys. Chem. B*, 2004, **108**, 8614–8621.
36 Y. X. Zhang, X. Cai, Y. Z. Bian, X. Y. Li and J. Z. Jiang, *J. Phys. Chem. C*, 2008, **112**, 5148–5159.
37 G. R. Hutchison, M. A. Ratner and T. J. Marks, *J. Am. Chem. Soc.*, 2005, **127**, 2339–2350.
38 M. Y. Kuo, H. Y. Chen and I. Chao, *Chem.–Eur. J.*, 2007, **13**, 4750–4758.
39 L. Tan, L. Zhang, X. Jiang, X. D. Yang, L. J. Wang, Z. H. Wang, L. Q. Li, W. P. Hu, Z. Shuai, L. Li and D. B. Zhu, *Adv. Funct. Mater.*, 2009, **19**, 272–276.
40 G. J. Nan, L. J. Wang, X. D. Yang, Z. Shuai and Y. Zhao, *J. Chem. Phys.*, 2009, **130**, 024704.
41 J. Bisquert, *Phys. Chem. Chem. Phys.*, 2008, **10**, 3175–3194.
42 R. A. Marcus, *Rev. Mod. Phys.*, 1993, **65**, 599–610.
43 G. R. Hutchison, M. A. Ratner and T. J. Marks, *J. Am. Chem. Soc.*, 2005, **127**, 16866–16881.
44 X. Y. Li, *J. Comput. Chem.*, 2001, **22**, 565–579.
45 E. F. Valeev, V. Coropceanu, D. A. da Silva Filho, S. Salman and J.-L. Brédas, *J. Am. Chem. Soc.*, 2006, **128**, 9882–9886.
46 A. Troisi and G. Orlandi, *J. Phys. Chem. B*, 2002, **106**, 2093–2101.
47 M. J. Frisch, G. W. Trucks, H. B. Schlegel, G. E. Scuseria, M. A. Robb, J. R. Cheeseman, J. A. Montgomery, Jr, T. Vreven, K. N. Kudin, J. C. Burant, J. M. Millam, S. S. Iyengar, J. Tomasi, V. Barone, B. Mennucci, M. Cossi, G. Scalmani, N. Rega, G. A. Petersson, H. Nakatsuji, M. Hada, M. Ehara, K. Toyota, R. Fukuda, J. Hasegawa, M. Ishida, T. Nakajima, Y. Honda, O. Kitao, H. Nakai, M. Klene, X. Li, J. E. Knox, H. P. Hratchian, J. B. Cross, V. Bakken, C. Adamo, J. Jaramillo, R. Gomperts, R. E. Stratmann, O. Yazyev, A. J. Austin, R. Cammi, C. Pomelli, J. W. Ochterski, P. Y. Ayala, K. Morokuma, G. A. Voth, P. Salvador, J. J. Dannenberg, V. G. Zakrzewski, S. Dapprich, A. D. Daniels, M. C. Strain, O. Farkas, D. K. Malick, A. D. Rabuck, K. Raghavachari, J. B. Foresman, J. V. Ortiz, Q. Cui, A. G. Baboul, S. Clifford, J. Cioslowski, B. B. Stefanov, G. Liu, A. Liashenko, P. Piskorz, I. Komaromi, R. L. Martin, D. J. Fox, T. Keith, M. A. Al-Laham, C. Y. Peng, A. Nanayakkara, M. Challacombe, P. M. W. Gill, B. Johnson, W. Chen, M. W. Wong, C. Gonzalez and J. A. Pople, *Gaussian 0.3 (Revision C.02)*, Gaussian Inc., Wallingford, CT, 2004.
48 M. Kitamura and Y. Arakawa, *J. Phys.: Condens. Matter*, 2008, **20**, 184011.
49 J.-L. Brédas, J. P. Calbert, D. A. da Silva Filho and J. Cornil, *Proc. Natl. Acad. Sci. U. S. A.*, 2002, **99**, 5804–5809.
50 J. Cornil, V. Lemaur, J. P. Calbert and J.-L. Brédas, *Adv. Mater.*, 2002, **14**, 726–729.
51 V. Lemaur, D. A. da Silva Filho, V. Coropceanu, M. Lehmann, Y. Geerts, J. Piris, M. G. Debije, A. M. van de Craats, K. Senthilkumar, L. D. A. Siebbeles, J. M. Warman, J.-L. Brédas and J. Cornil, *J. Am. Chem. Soc.*, 2004, **126**, 3271–3279.
52 J. E. Norton and J.-L. Brédas, *J. Chem. Phys.*, 2008, **128**, 034701.
53 J. E. Anthony, *Chem. Rev.*, 2006, **106**, 5028–5048.
54 J. E. Anthony, *Angew. Chem., Int. Ed.*, 2008, **47**, 452–483.
55 L. Antolini, G. Horowitz, F. Kouki and F. Garnier, *Adv. Mater.*, 1998, **10**, 382–385.
56 T. Siegrist, C. Kloc, R. A. Laudise, H. E. Katz and R. C. Haddon, *Adv. Mater.*, 1998, **10**, 379–382.
57 T. Siegrist, R. M. Fleming, R. C. Haddon, R. A. Laudise, A. J. Lovinger, H. E. Katz, P. Bridenbaugh and D. D. Davis, *J. Mater. Res.*, 1995, **10**, 2170–2173.
58 G. Horowitz, B. Bachet, A. Yassar, P. Lang, F. Demanze, J. L. Fave and F. Garnier, *Chem. Mater.*, 1995, **7**, 1337–1341.
59 M. Mas-Torrent, P. Hadley, S. T. Bromley, X. Ribas, J. Tarrés, M. Mas, E. Molins, J. Veciana and C. Rovira, *J. Am. Chem. Soc.*, 2004, **126**, 8546–8553.
60 S. H. Lin, C. H. Chang, K. K. Liang, R. Chang, Y. J. Shiu, J. M. Zhang, T. S. Yang, M. Hayashi and F. C. Hsu, *Adv. Chem. Phys.*, 2002, **121**, 1–88.
61 M. Bixon and J. Jortner, *J. Phys. Chem.*, 1991, **95**, 1941–1944.
62 L. B. Schein, C. B. Duke and A. R. McGhie, *Phys. Rev. Lett.*, 1978, **40**, 197–200.
63 W. H. Miller, S. D. Schwartz and J. W. Tromp, *J. Chem. Phys.*, 1983, **79**, 4889–4898.
64 C. Y. Zhu and H. Nakamura, *J. Chem. Phys.*, 1994, **101**, 10630–10647.
65 Y. Zhao, W. Z. Liang and H. Nakamura, *J. Phys. Chem. A*, 2006, **110**, 8204–8212.
66 Y. Zhao, T. Yamamoto and W. H. Miller, *J. Chem. Phys.*, 2004, **120**, 3100–3107.
67 L. J. Wang, Q. K. Li, Z. Shuai, L. P. Chen and Q. Shi, *Phys. Chem. Chem. Phys.* in revision.
68 G. M. Day, T. G. Cooper, A. J. Cruz-Cabeza, K. E. Hejczyk, H. L. Ammon, S. X. M. Boerrigter, J. S. Tan, R. G. Della Valle, E. Venuti, J. Jose, S. R. Gadre, G. R. Desiraju, T. S. Thakur, B. P. van Eijck, J. C. Facelli, V. E. Bazterra, M. B. Ferraro, D. W. M. Hofmann, M. A. Neumann, F. J. J. Leusen, J. Kendrick, S. L. Price, A. J. Misqutta, P. G. Karamertzanis, G. W. A. Welch, H. A. Scheraga, Y. A. Arnautova, M. U. Schmidt, J. van de Streek, A. K. Wolf and B. Schweizer, *Acta Crystallogr., Sect. B: Struct. Sci.*, 2009, **65**, 107–125.
69 H. B. Wang, X. Y. Song, D. Chandler and W. H. Miller, *J. Chem. Phys.*, 1999, **110**, 4828–4840.
70 M. H. Beck, A. Jäckle, G. A. Worth and H.-D. Meyer, *Phys. Rep.*, 2000, **324**, 1–105.
71 M. Topaler and N. Makri, *J. Phys. Chem.*, 1996, **100**, 4430–4436.
72 J. M. Jean, R. A. Friesner and G. R. Fleming, *J. Chem. Phys.*, 1992, **96**, 5827–5842.
73 A. Troisi, *Adv. Mater.*, 2007, **19**, 2000–2004.